Atomic Force Microscopy of Crystalline Insulins: The Influence of Sequence Variation on Crystallization and Interfacial Structure

Christopher M. Yip,* Mark L. Brader,* Michael R. DeFelippis,* and Michael D. Ward#
*Lilly Research Laboratories, Eli Lilly and Company, Indianapolis, Indiana 46285, and #Department of Chemical Engineering and Materials Science and the Center for Interfacial Engineering, University of Minnesota, Minneapolis, Minnesota 55455 USA

ABSTRACT The self-association of proteins is influenced by amino acid sequence, molecular conformation, and the presence of molecular additives. In the presence of phenolic additives, $Lys^{B28}Pro^{B29}$ insulin, in which the C-terminal prolyl and lysyl residues of wild-type human insulin have been inverted, can be crystallized into forms resembling those of wild-type insulins in which the protein exists as zinc-complexed hexamers organized into well-defined layers. We describe herein tapping-mode atomic force microscopy (TMAFM) studies of single crystals of rhombohedral (R3) $Lys^{B28}Pro^{B29}$ that reveal the influence of sequence variation on hexamer-hexamer association at the surface of actively growing crystals. Molecular scale lattice images of these crystals were acquired in situ under growth conditions, enabling simultaneous identification of the rhombohedral $Lys^{B28}Pro^{B29}$ crystal form, its orientation, and its dynamic growth characteristics. The ability to obtain crystallographic parameters on multiple crystal faces with TMAFM confirmed that bovine and porcine insulins grown under these conditions crystallized into the same space group as $Lys^{B28}Pro^{B29}$ (R3), enabling direct comparison of crystal growth behavior and the influence of sequence variation. Real-time TMAFM revealed hexamer vacancies on the (001) terraces of $Lys^{B28}Pro^{B29}$, and more rounded dislocation noses and larger terrace widths for actively growing screw dislocations compared to wild-type bovine and porcine insulin crystals under identical conditions. This behavior is consistent with weaker interhexamer attachment energies for $Lys^{B28}Pro^{B29}$ at active growth sites. Comparison of the single crystal x-ray structures of wild-type insulins and $Lys^{B28}Pro^{B29}$ suggests that differences in protein conformation at the hexamer-hexamer interface and accompanying changes in interhexamer bonding are responsible for this behavior. These studies demonstrate that subtle changes in molecular conformation due to a single sequence inversion in a region critical for insulin self-association can have a significant effect on the crystallization of proteins.

INTRODUCTION

Insulin is a small, 51-amino acid, dual-chain hormone produced in the pancreas that plays a crucial role in the maintenance of blood glucose levels. The inability to achieve glucose homeostasis leads to the development of diabetes, a chronic disease that often requires supplemental insulin in the form of regular injections of either freely soluble insulin or microcrystalline insulin suspensions. The efficacy of such therapies strongly depends upon the dissociation of insulin hexamers to the bioactive monomers (Hollenberg, 1990; Gammeltoft, 1988; Berson and Yalow, 1966; Smith et al., 1984). In the case of microcrystalline insulin suspensions, the efficacy is also influenced by the rate of crystal dissolution, which depends on crystal structure (polymorphism), morphology, and size. However, numerous single crystal structural investigations of insulin reveal that this protein crystallizes as layers of hexamer units. This suggests that a crucial first step in crystal dissolution is disruption of the hexamer-hexamer interface at the crystal surface.

One approach to the development of insulin therapies relies on controlling insulin self-association by specific alterations to the sequence of wild-type human insulin (Brems et al., 1992a,b; Brange et al., 1990, 1991). The synthesis of $Lys^{B28}Pro^{B29}$, an insulin analog in which the prolyl and lysyl residues at positions 28 and 29 in the B-chain of wild-type human insulin are inverted, is illustrative of such efforts (DiMarchi et al., 1992; Long et al., 1992; Howey et al., 1994). This minor sequence inversion, which occurs in the region of the insulin B-chain known to be involved in dimer formation, yields a bioactive insulin analog whose self-association equilibria are shifted strongly toward the monomer, in contrast to the wild types that exist predominantly as hexamers. Nevertheless, recent x-ray diffraction studies performed on single crystals of $Lys^{B28}Pro^{B29}$ grown in the presence of phenol, which was required for isolation of x-ray quality crystals, revealed that the $Lys^{B28}Pro^{B29}$ monomers assemble as zinc-complexed hexamers, despite the reduced association constant of the hexamer (Ciszak et al., 1995).

The phenolic additives apparently stabilize the $Lys^{B28}Pro^{B29}$ hexamer so that crystallization, via self-assembly of hexamer units, can occur. The dissolution characteristics of crystalline forms of $Lys^{B28}Pro^{B29}$ will depend upon the detachment of hexamers from exposed crystal surfaces, typically at high surface energy sites such as steps and kinks. Consequently, the role of the sequence inversion and accompanying conformational perturbation to hexamer-

Received for publication 24 September 1997 and in final form 8 February 1998.

Address reprint requests to Dr. Michael R. DeFelippis, Lilly Research Laboratories, Eli Lilly and Company, Indianapolis, IN 46285. Tel.: 317-276-6027; Fax: 317-277-0833; E-mail: defelippis_michael_r@lilly.com; or to Prof. Michael D. Ward, Department of Chemical Engineering and Materials Science, University of Minnesota, 421 Washington Ave SE, Minneapolis, MN 55455. Tel.: 612-625-3062; Fax: 612-626-7246; E-mail: wardx0001@maroon.tc.umn.edu.

0006-3495/98/05/2199/11 $2.00

hexamer self-association in the crystal needs to be elucidated. This requires direct experimental observation of phenomena related to hexamer-hexamer association coupled with analysis of the hexamer-hexamer interface. This prompted us to examine the structure and growth characteristics of $Lys^{B28}Pro^{B29}$ crystals with real-time in situ atomic force microscopy (AFM). Several recent investigations have demonstrated that AFM is ideal for examining crystallization, at the near-molecular level, of small-molecule organic crystals (Manne et al., 1993; Last and Ward, 1996; Hillier and Ward, 1994; Hillier et al., 1994; Carter et al., 1994; Mao et al., 1997) and protein crystals (Ng et al., 1997; Yip and Ward, 1996; McPherson et al., 1996; Kuznetsov et al., 1996; Land et al., 1995, 1996; Malkin et al., 1995; Konnert et al., 1994; Durbin et al., 1993; Durbin and Carlson, 1992). This method enables direct assignment of the crystal planes under investigation, observation of defects, characterization of the topography (i.e., steps, ledges, kinks) of actively growing faces, determination of the influence of additives on topography, and measurement of crystallization rates along specific crystallographic directions. We describe herein AFM investigations that reveal differences in specific crystal growth characteristics of $Lys^{B28}Pro^{B29}$ and wild-type insulins that reflect weaker interhexamer interactions in the former. Comparison of the crystal structures of the two forms reveals differences in conformation and intermolecular interactions at the hexamer-hexamer interface that may be responsible for this behavior. These observations are quite remarkable in that they illustrate the extent to which a single sequence inversion can perturb the delicate noncovalent interactions responsible for hexamer-hexamer association at the crystal surface, and the influence of the perturbations on crystal growth, crystal dissolution, and crystal quality. Furthermore, these results illustrate that AFM performed on crystal surfaces can provide direct insight into the nature of insulin self-association in different crystalline formulations, which is crucial for elucidating the therapeutic efficacy of the treatment of diabetes.

MATERIALS AND METHODS

Crystals of $Lys^{B28}Pro^{B29}$ insulin were prepared by the following procedure, which has been described previously (Ciszak et al., 1995). To a precleaned 20-ml glass scintillation vial containing 10 mg of $Lys^{B28}Pro^{B29}$ (Eli Lilly and Company) was added 5 ml of 0.02 M HCl. After gentle swirling to dissolve the $Lys^{B28}Pro^{B29}$, 12 μl of aqueous 20 weight % $ZnCl_2$, 16.5 μl of aqueous 90 weight % phenol, and 2 ml of 0.2 M sodium citrate buffer were added sequentially to afford a slightly turbid solution. After adjusting the pH of the solution to ~5.7, the solution was heated gently to 50°C in a water bath to afford a clear solution. Slow cooling of this solution to room temperature over several days afforded well-defined micron-sized crystals. Crystals of recombinant human and purified bovine and porcine insulins (Eli Lilly and Company) were prepared under identical conditions.

Solution tapping-mode AFM (TMAFM) images were acquired with a Digital Instruments Nanoscope III MultiMode scanning probe microscope with a combination contact/tapping-mode liquid cell (Digital Instruments, Santa Barbara, CA). All images were acquired using 120-μm oxide-sharpened silicon nitride V-shaped cantilevers with integral bipyramidal tips (type DNP-S; Digital Instruments). Before use, the AFM tips were exposed to UV irradiation to remove adventitious organic contaminants from the tip surface. It should be noted that tapping-mode operation in solution employs cantilevers with a lower spring constant than is typically employed for tapping mode in air, to compensate for viscous coupling between the cantilever and surrounding fluid that increases the effective spring constant of the cantilever. AFM images were acquired using a scanning head with a maximum lateral scan area of 14.6 μm × 14.6 μm. The crystals to be examined were transferred via pipette into a well formed by an O-ring affixed to an AFM sample mount coated with a thin layer of vacuum grease. The lateral translation of the AFM tip is restricted by the O-ring in this configuration, thereby hampering the positioning of the tip on a sample region of interest. Consequently, it was important to devise a procedure that enabled reliable positioning of the tip on an insulin crystal. This was accomplished by mounting the cantilever into the body of the AFM liquid cell and aligning the laser spot on the cantilever tip without a sample present. The liquid cell then was removed from the AFM optical head and replaced with the AFM sample mount to which the crystals were affixed. Without adjusting the laser spot positioning screws and while monitoring the position of the laser spot through an optical microscope, the AFM optical head was translated in the *x-y* plane until the laser spot was located above a crystal of interest. The liquid cell body containing the inserted cantilever tip was then reseated over the O-ring. This procedure also reduced sample creep arising from relaxation of the O-ring.

Stable images were acquired at cantilever drive frequencies ranging from 6 to 30 kHz, but imaging was optimal at frequencies near 8.9 kHz. However, a priori determination of the appropriate drive frequency was difficult, owing to viscous coupling between the cantilever and the fluid medium, which gave rise to multiple broad resonance peaks. The range and selection of optimal imaging drive frequencies were somewhat dependent on the particular cantilever, sample surface, and solution conditions. The cantilever drive voltage and setpoint imaging voltage significantly influenced image quality and sample integrity, and occasional slight departures from optimum values resulted in sample etching. Accordingly, feedback conditions were selected based on optimization of image quality. Data analyses were performed on low-pass filtered AFM images, using Nanoscope III (version 4.22b1; Digital Instruments) and National Institutes of Health Image (version 1.61) software packages. National Institutes of Health Image is available by anonymous file transfer protocol from zippy.nimh.nih.gov.

RESULTS AND DISCUSSION

Crystallographic characterization by AFM

The $Lys^{B28}Pro^{B29}$ insulin molecule differs from its human, bovine, and porcine wild-type analogs by a sequence inversion of the proline and lysine residues at positions 28 and 29 in the C-terminus of the B-chain, and substitution of alanine for threonine in the case of bovine and porcine insulin (Table 1). Using established procedures, crystals of $Lys^{B28}Pro^{B29}$ were grown from solution as the rhombohedral form (Ciszak et al., 1995). Under identical growth conditions, crystals of wild-type human, bovine, and porcine insulins grew as thick rectangular plates. The crystal structures have been reported for wild-type human and

TABLE 1 Comparison of the sequence in the C-terminus of the B-chain for wild-type and $Lys^{B28}Pro^{B29}$ insulins

Residue number:	**23**	**24**	**25**	**26**	**27**	**28**	**29**	**30**
Human:	Gly	Phe	Phe	Tyr	Thr	Pro	Lys	**Thr**
Bovine/porcine:	Gly	Phe	Phe	Tyr	Thr	Pro	Lys	**Ala**
$Lys^{B28}Pro^{B29}$:	Gly	Phe	Phe	Tyr	Thr	**Lys**	**Pro**	Thr

porcine insulins, but the structures of crystals grown under the conditions used here are unknown (although it is unlikely that the crystal structures would be dramatically affected by these conditions).

Tapping mode AFM (TMAFM) images of the largest face of the $Lys^{B28}Pro^{B29}$ single crystals were acquired directly in the crystallization liquor. The tapping mode (Hansma et al., 1994) was used because conventional contact mode caused significant etching of the crystal surfaces. The AFM images of this face revealed large, molecularly smooth, micron-sized terraces decorated by steps with heights of ~30 Å. This step height is similar to the value of the c lattice constant of rhombohedral $Lys^{B28}Pro^{B29}$ (space group R3, $a = b = 79.62$ Å, $c = 37.78$ Å, $\gamma = 120°$, as indexed on hexagonal axes). This suggested that the imaged face was (001), which, based on single crystal x-ray diffraction (Ciszak et al., 1995), can be described as a corrugated layer of insulin hexamers arranged in a hexagonal motif. The 30-Å step heights observed by AFM were somewhat smaller than expected, based on the c lattice constant. This may be due to differences in solvation between $Lys^{B28}Pro^{B29}$ hexamer layers at the crystal-solution interface and in the bulk crystal. The assignment of this face as (001) was confirmed by TMAFM images acquired in the crystallization liquor over a smaller region of the face. These images revealed molecular-level contrast of a nominally hexagonal 2-D lattice (Fig. 1) with 2-D lattice constants, as determined from the real space AFM data and the corresponding two-dimensional Fourier power spectrum, $a_1 = 43.4$ Å ± 4 Å, $a_2 = 48.5$ Å ± 4 Å, $a_3 = 52.0$ Å ± 5 Å, $\gamma_{12} = 53.3°$, and $\gamma_{23} = 68.1°$. The averages of these values ($a_1 = 48.0$ Å; $\gamma_{12} = 60.8°$) are in good agreement with the symmetry and periodicity expected ($a_1 = 46.0$ Å and $\gamma_{12} = 60°$) for the hexagonal arrangement of the insulin hexamers when viewed normal to the (001) plane, as depicted in Fig. 1 *B*. The slight departure of the AFM data from a perfect hexagonal arrangement can be attributed to intrinsic measurement error. The 46-Å a_1 lattice constant (equivalent to a_2 and a_3) represents the separation between hexamers along the close-packed directions in the (001) plane. Close inspection of the lattice images acquired on adjacent terraces separated by steps revealed excellent translational and rotational registry between overlying (001) layers, indicating the structural order required for good crystal quality. This confirms the R3 rhombohedral phase, in which the hexagonal arrays are stacked in registry along the c axis.

The single crystal x-ray structures of human, bovine, and porcine insulins prepared under the conditions described in Materials and Methods have not been reported. To compare the crystal growth characteristics of the R3 $Lys^{B28}Pro^{B29}$ insulin with other wild types, it was important to verify that

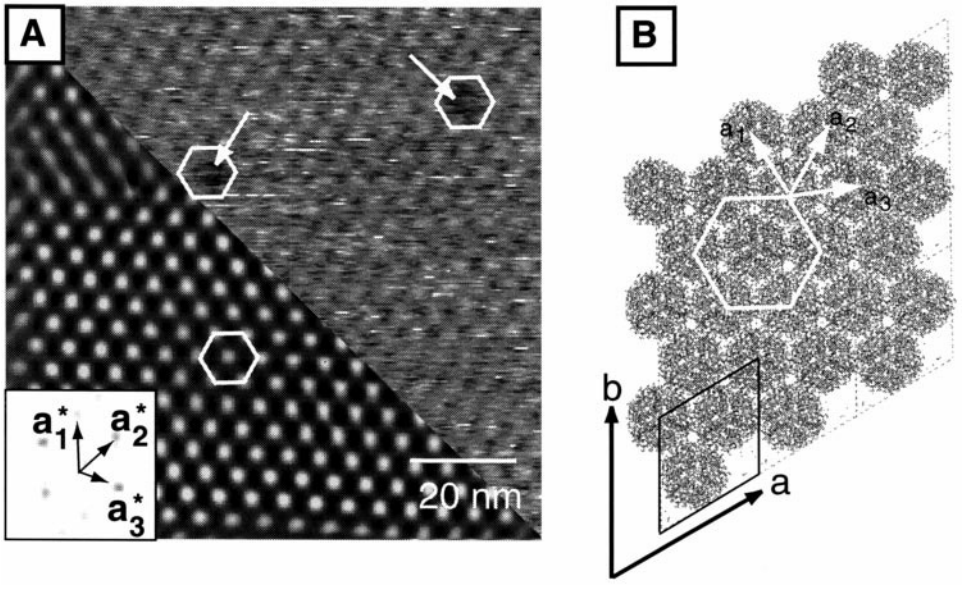

FIGURE 1 (*A*) Real space TMAFM lattice image, obtained in situ during crystallization, for the (001) crystal plane of $Lys^{B28}Pro^{B29}$. Scan size = 100 nm × 100 nm; scan rate = 4.36 Hz. Raw and Fourier filtered data are displayed in the upper right and lower left regions of the image. The hexagonal symmetry apparent in this data corresponds to the arrangement of insulin hexamers in the (001) plane. (*Inset*) The two-dimensional Fourier power spectrum corresponding to the AFM data. The reciprocal lattice vectors describe a hexagonal 2-D lattice with $a_1 = 43.4$ Å; $a_2 = 48.5$ Å; $a_3 = 52.0$ Å; $\gamma_{12} = 53.3°$; $\gamma_{23} = 68.1°$, as depicted here by the alternative hexagonal lattice. The average of these values ($a_1 = 48.0$ Å; $\gamma_{12} = 60.8°$) is in good agreement with the nearest neighbor hexamer separation ($a_1 = 46.0$ Å) and the hexagonal symmetry of the (001) layers ($\gamma = 60°$). The real space vectors a_1, a_2, and a_3 define the nearest neighbor packing of the hexamers. The arrows on the raw data in *A* indicate vacancies in the (001) crystal plane corresponding to missing $Lys^{B28}Pro^{B29}$ hexamers. (*B*) The $Lys^{B28}Pro^{B29}$ hexamer packing motif of the (001) plane based on single crystal x-ray diffraction. The rhombohedral unit cell used for the structure solution is depicted by the solid black lines, with $a = b = 79.62$ Å and $c = 37.78$ Å, indexed on hexagonal axes. The structural model in *B* was prepared with Cerius^2 version 2.0 (Molecular Simulations, San Diego, CA), using coordinates registered with the Brookhaven Protein Data Bank as pdb1lph.ent.

the wild-type crystalline forms grown under these conditions crystallized in the same space group as $Lys^{B28}Pro^{B29}$. Notably, 65% of the insulin structures for which space groups have been assigned in the Brookhaven Protein Database belong to the R3 space group, compared to only 2% of all crystal structures in the Database (Abola et al., 1987; Bernstein et al., 1977). Indeed, the R3 space group was corroborated for bovine insulin crystals by lattice images acquired with in situ TMAFM on single crystals that were tilted so that crystallographically different adjoining faces were accessible to the TMAFM tip in a single experiment (Fig. 2 *A*). TMAFM images acquired on the large terraces of the screw dislocation in region 1 of Fig. 2 *A* exhibited nominally hexagonal symmetry, with $a_1 = 43$ Å $\pm$ 4 Å and $\gamma = 62° \pm 4°$, in good agreement with the values expected for the (001) crystal plane of the R3 insulin. In contrast, images acquired on the large terraces of the screw dislocation in region 2 afforded a monoclinic lattice with $a_1 = 33.5$ Å $\pm$ 3 Å, $a_2 = 45.1$ Å $\pm$ 4 Å, and $\gamma = 60° \pm 3°$. These values are in good agreement with those expected for the monoclinic arrangement of insulin hexamers on the (110) plane of the rhombohedral cell used for structure solution, for which values of $a_1 = 37.8$ Å, $a_2 = 47.7$ Å, and $\gamma = 61°$ are expected. Attempts to obtain molecular-scale lattice images on porcine insulin grown under the same conditions were not successful, owing to the difficulties in locating a properly oriented crystal. However, the (001) lattice images, surface features, and morphology of the porcine crystals determined by AFM were identical to those of the bovine and $Lys^{B28}Pro^{B29}$ insulin crystals. This argues that all three insulins grown under these conditions crystallized in the R3 space group. These results demonstrate the crystallographic capabilities of in situ AFM with respect to screening possible space group symmetries for protein crystals that have not been characterized by single-crystal x-ray diffraction.

Crystal defects

The TMAFM images revealed numerous vacancies on the $Lys^{B28}Pro^{B29}$ (001) terraces that were not present on the wild-type bovine, porcine, and human insulin crystals. These vacancies exhibited sizes corresponding to the absence of single hexamers or multiples of hexamers (Fig. 1 *A*). The defects were stable on the AFM time scale, and additional ones were not formed upon prolonged scanning, indicating that their formation was not a consequence of the tapping-mode imaging process. Although detection of sin-

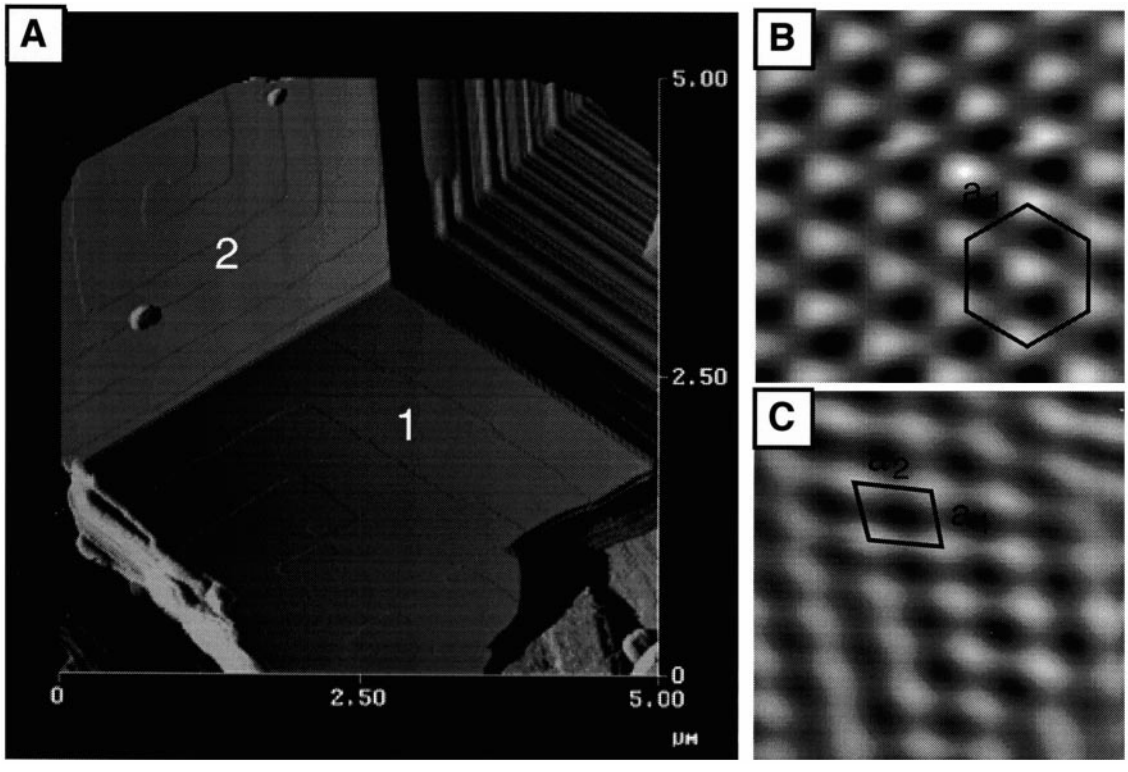

FIGURE 2 (*A*) In situ AFM tapping mode image acquired across the intersection of three crystal faces of a bovine insulin crystal grown under the same conditions as used for crystallization of $Lys^{B28}Pro^{B29}$ insulin. Scan size = 5 μm $\times$ 5 μm; scan rate = 2.00 Hz. Well-defined screw dislocations are evident. (*B*) Lattice images acquired in region 1 and (*C*) in region 2. Scan size: 25 nm $\times$ 25 nm; scan rate: 2.00 Hz. The two-dimensional unit cells, determined from the respective Fourier power spectra, are outlined in black. The hexagonal lattice in region 1 and the monoclinic lattice in region 2 are consistent with the arrangement of insulin hexamers on the (001) and (110) planes of the R3 rhombohedral cell. Experimental lattice parameters: region 1: $a_1 = 43$ Å $\pm$ 4 Å; $\gamma = 62° \pm 4°$; region 2: $a_1 = 33.5$ Å $\pm$ 3 Å; $a_2 = 45.1$ Å $\pm$ 4 Å; $\gamma = 60° \pm 3°$. Expected values based on R3 $Lys^{B28}Pro^{B29}$ insulin: (001): $a_1 = 46.0$ Å Å; $\gamma = 60°$; (110): $a_1 = 37.8$ Å; $a_2 = 47.7$ Å; $\gamma = 61°$.

gle atomic- or molecular-scale defects generally is difficult owing to the ensemble imaging mechanism of the AFM, in the case of $Lys^{B28}Pro^{B29}$, a single hexamer defect would be ~5 nm in diameter, which is within the resolution limits of the TMAFM.

Sampling of numerous (001) $Lys^{B28}Pro^{B29}$ crystal terraces revealed that the defect density was $\sim 10^{10}$ cm^{-2}, which was several orders of magnitude larger than values reported for other protein systems such as thaumatin (10^4-10^6 defects $\cdot$ cm^{-2}) (Malkin et al. 1996). It has been suggested that the requirement of phenolic additives for the crystallization of $Lys^{B28}Pro^{B29}$ and the absence of directed bonding interactions from the conformationally flexible N-terminal regions of the B-chain in the interhexamer contact region are evidence of weaker interhexamer interactions for $Lys^{B28}Pro^{B29}$ compared to the wild-type insulin forms (Bakaysa et al., 1996; Birnbaum et al., 1997; Ciszak et al., 1995). This argues that the point defects are due to detachment of hexamers from the crystal surface layer. Vacancy formation during growth is also possible. As the monomer-monomer association constant for $Lys^{B28}Pro^{B29}$ is significantly lower than for wild-type human insulin, with correspondingly lower equilibrium constants for higher even-order aggregates (Brems et al., 1992a), nonspecific attachment of subhexamer aggregates to the growing crystal surfaces may induce vacancy formation.

Our AFM studies also revealed random features on the (001) terraces of the $Lys^{B28}Pro^{B29}$ and the wild-type insulin crystals that are similar to features observed on bovine insulin in a previous study in our laboratory (Yip and Ward, 1996). The dimensions of these features were ~20 nm $\times$ ~10 nm $\times$ ~2.5 nm. These were presumed to be insulin aggregates that have attached to the surface after formation in solution or aggregates formed by Ostwald ripening on the crystal surface. The former is supported by previous studies that have confirmed the presence of insulin aggregates in solution before crystallization (Milthorpe et al., 1977; Bohinder and Geissler, 1984; Pederson et al., 1994; Jeffrey, 1974; Hvidt, 1991). We have not observed any evidence for diffusion of these aggregates along the surface to an actively growing step on the time scale of our AFM imaging. The poor mobility of the large aggregates actually instigates the formation of macroscopic defects such as dislocation cores and voids in individual terraces (see *box*, Fig. 3, *D–F*). Advancing steps grew around the aggregate, leaving a depletion zone between the aggregate and the step edge. An examination of numerous $Lys^{B28}Pro^{B29}$ and wild-type insulin single crystals by tapping-mode AFM in solution revealed similar voids at the center of several screw dislocations, suggesting that these aggregates may initiate screw dislocations. Similar behavior has been reported previously (Yip and Ward, 1996; Malkin et al., 1996; Land et al., 1996). The persistence of these defects contrasts with the repair of large surface defects formed by mechanical etching with the AFM tip. Repair of these defects occurred at a rate comparable to that of step advancement, with volume growth rates of 1.1×10^{-6} $\mu m^3 \cdot s^{-1}$ and 2×10^{-6} $\mu m^3 \cdot s^{-1}$, respectively (volume growth rates were used for comparison purposes because the mechanically etched region was nominally three molecular layers deep, whereas the screw dislocation and terrace expansion regions comprised only single molecular terraces). These growth rates correspond to the attachment of approximately five unit cells (15 $Lys^{B28}Pro^{B29}$ hexamers) per second. Growth in the etched region occurred by expansion of individual terrace edges, with the lowest terraces filling first. These data suggest well-ordered repair of the surface via attachment of

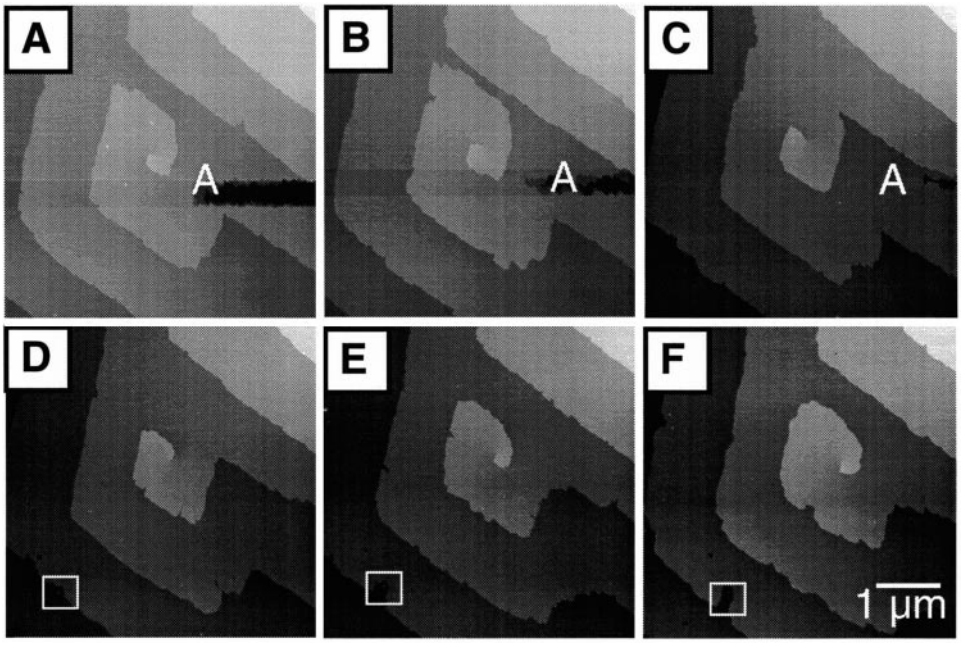

FIGURE 3 (*A–F*) In situ real-time solution tapping mode AFM images of the (001) plane of a $Lys^{B28}Pro^{B29}$ single crystal. Images were acquired at (*A*) 0, (*B*) 3605, (*C*) 7210, (*D*) 10,815, (*E*) 18,025, and (*F*) 40,590 s. Scan size = 5 μm $\times$ 5 μm; scan rate = 2.00 Hz. The rectangular area marked A corresponds to a region that was mechanically etched by the AFM tip during imaging. The screw dislocation completes a rotation during the image sequence. The etched region refills within 120 min to generate a fully repaired terrace surface. In *D*, a protein aggregate, outlined by a white box, has attached to the crystal surface. In *E* and *F*, this aggregate has not been incorporated into the growing step edge, but rather instigates the formation of a depletion zone that creates a persistent defect in the (001) layer.

hexamers to the advancing step edges and the absence of large aggregates on the terraces that would impede growth.

Crystal growth, including protein crystal growth, predominantly occurs by either two-dimensional nucleation or screw dislocation-driven growth. The prominent crystal faces of both the $Lys^{B28}Pro^{B29}$ and wild-type insulins exhibited well-defined screw dislocations under the conditions employed here. Real-time in situ TMAFM on the (001) plane revealed layer-by-layer growth in which the layers were spawned from the screw dislocations (Fig. 3). Interestingly, this contrasts with previous studies of bovine insulin crystal growth under different conditions (Yip and Ward, 1996), in which screw dislocations were never observed. This demonstrates that screw dislocation density can be very sensitive to growth conditions. It is also important to note that we did not observe tip-induced nucleation or enhanced crystal growth within the imaged region that may result from increased convection in the immediate vicinity of the imaging region (LaGraff and Gewirth, 1994, 1995; Land et al., 1996). This argues that crystal growth is dictated by surface diffusion to the growing step edge, as opposed to bulk volume diffusion to the crystal-solution interface (Yip and Ward, 1996). The crystal structures of both the wild-type and the $Lys^{B28}Pro^{B29}$ insulins indicate that the hexamer is the basic structural unit, which argues that the hexamer is the fundamental growth unit attaching to steps on the (001) face (Kadima et al., 1991; Baker et al., 1988). Preliminary light scattering data acquired in our laboratory during $Lys^{B28}Pro^{B29}$ crystallization are also consistent with this view.

Complex interlinked screw dislocations were observed occasionally on the $Lys^{B28}Pro^{B29}$ and wild-type human, bovine, and porcine insulin crystals (Fig. 4). One such complex dislocation on the (001) surface of a porcine insulin single crystal featured both left- and right-handed screw dislocations that can be described as a Frank-Read dislocation loop (Fig. 4 *A*). These data illustrate the correspondence of the screw dislocations crystal structure and bulk crystal morphologies. The intersecting steps subtend an angle of 125°, in good agreement with the 120° angle subtended by the [110] and [$1\bar{1}$ 0] directions, which define the nearest-neighbor interhexamer contacts.

Comparison of the screw dislocations on actively growing (001) faces of $Lys^{B28}Pro^{B29}$, porcine, and bovine crystals reveals obvious differences in the curvature of the dislocation noses (i.e., the region of intersection of two steps) and in the terrace widths (which correspond to the ledge wavelength, λ_1). Specifically, the terrace widths and nose curvature are significantly larger for $Lys^{B28}Pro^{B29}$ than for porcine and bovine insulin. These topographical features, which represent the nanoscale origins of the bulk crystal habit, stem from differences in surface energies and attachment free energies at the relevant crystal planes (Tiller, 1991, 1992). The nose radius of curvature (r_c), which is equivalent to the critical nuclei radius of a stable two-dimensional nucleus, is related to the surface energy of the dislocation ledge (γ_l) and the free energy of attachment at the kink sites on the ledges of the dislocation (ΔG_k) according to Eq. 1, and is related to λ_l according to Eq. 2:

$$r_c = \frac{\gamma_l}{\Delta G_k} \tag{1}$$

$$\lambda_l = 4\pi r_c = 4\pi \frac{\gamma_l}{\Delta G_k} \tag{2}$$

A rounded dislocation nose is the consequence of rough ledges (i.e., many kinks) and slow growth parallel to the ledge. Large values of γ_l will favor rough ledges and large terraces, because the overall surface energy will be reduced by reducing the total area of the step planes parallel to the ledge. Small values of ΔG_k are synonymous with low surface energies for the kink sites, which will favor the formation of these kink sites and roughening of the ledges. Similarly, large terrace widths (large λ_l) will be favored by small ΔG_k values, as the relative growth rate along the ledge direction will be smaller. Conversely, for a given γ_l, the net effect of a large ΔG_k is a screw dislocation with linear step edges and sharp corners. This is the behavior observed for the porcine insulin crystals (Fig. 3 *F*) and for the bovine crystals (not shown). In contrast, a larger radius of curvature and the development of capes and protrusions at the edges of the screw dislocation were observed for $Lys^{B28}Pro^{B29}$, indicating a smaller ΔG_k and/or a larger γ_l compared to porcine insulin (Fig. 3 *E*). Smaller ΔG_k values would be consistent with weaker interhexamer interactions, which has already been suggested as the source of the point defects described above.

The cohesive energies and the attachment energies for the $Lys^{B28}Pro^{B29}$ and the wild-type insulin crystals will be governed by solvent and noncovalent interactions in the region of interhexamer contact. The nature and availability of these interactions will be influenced by the conformation of the six monomer subunits of each hexamer, particularly by the sequences in the interhexamer contact region. The insulin monomer can adopt one of three conformations. In the T and R states, the residues B1–B8 (of the N-terminus of the B-chain) are in extended and α-helical conformations, respectively (Kaarsholm et al., 1989). In the "frayed" α-helix or R^f monomer state, the α-helix region is shorter, as residues B1 through B3 exist in an extended state (Ciszak et al., 1995). The $Lys^{B28}Pro^{B29}$ hexamer, which comprises three monomers in the T-state and three in the R^f state, can be described as a $T_3R_3^f$ hexamer.

The primary sequence differences for the wild-type human, bovine, and porcine insulins, and $Lys^{B28}Pro^{B29}$ insulin exist in the C-terminus of the B-chain (Table 1). To evaluate the effect of these sequence variations on interhexamer contacts, we compared the hexamer packing motifs in $Lys^{B28}Pro^{B29}$ (Brookhaven Protein Data Bank entry code: pdb1lph.ent) with the $T_3R_3^f$ human insulin structure (pdb1trz.ent; Ciszak and Smith, 1994) and the T_6 2-Zn porcine insulin structure (pdb4ins.ent), all of which belong to the R3 space group. The interhexamer contact region of

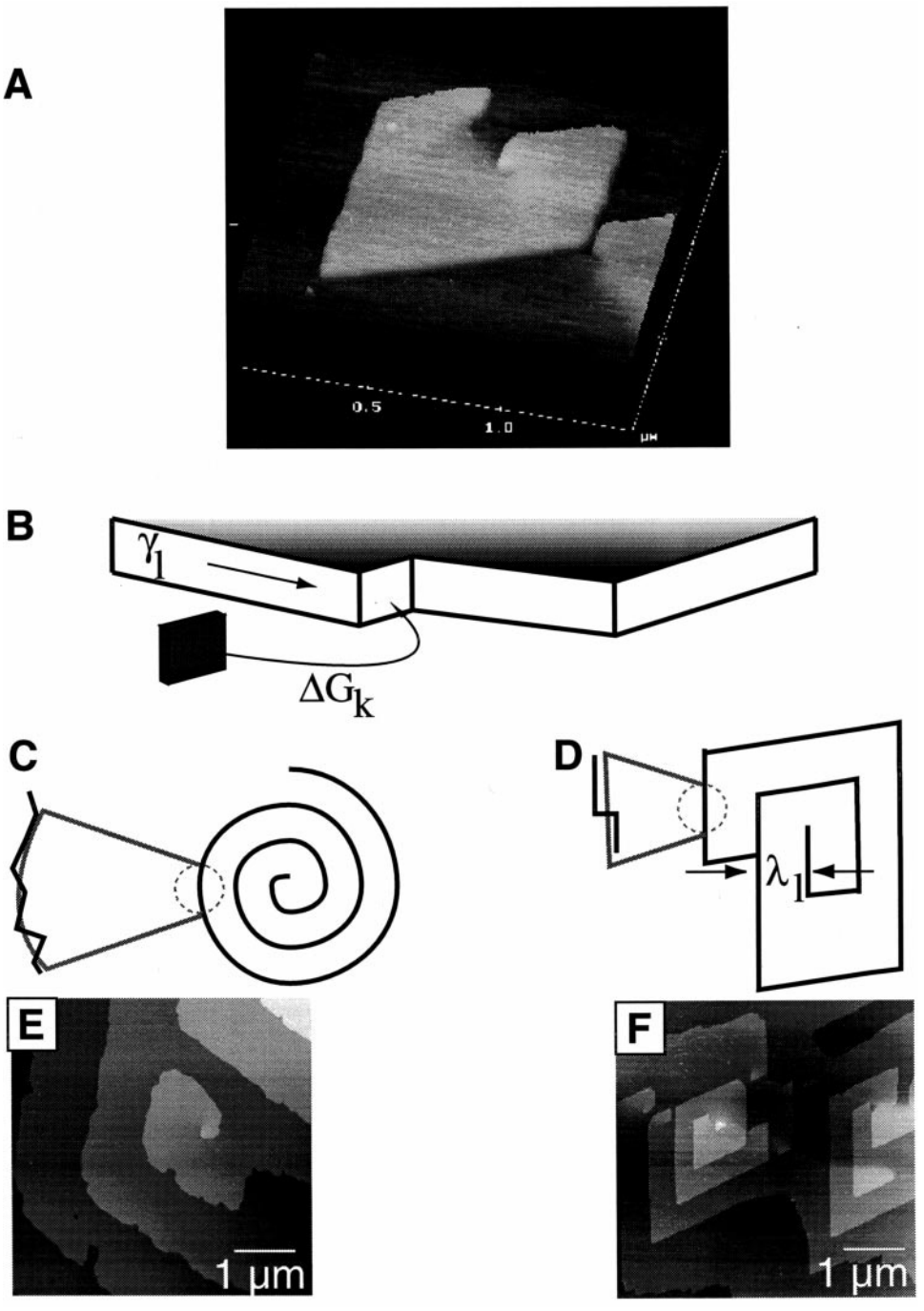

FIGURE 4 (*A*) In situ TMAFM image acquired during crystallization that illustrates a Frank-Read dislocation loop on the (001) crystal plane of a porcine insulin crystal grown under the conditions described in Materials and Methods. Scan size = 1.5 μm × 1.5 μm; scan rate = 2.0 Hz. The step height is ~38 Å. (*B*) Schematic representation of aggregate addition to a kink site on an exposed crystal terrace. The ledge interfacial energy and the free energy of kink addition are denoted by γ_l and ΔG_k, respectively. The width of the individual ledge sites is denoted by λ_l. (*C* and *D*) Schematic representations of (*C*) rounded and (*D*) sharp screw dislocations. The magnified regions illustrate that roughened ledges with numerous kink sites afford rounded dislocations, whereas smooth ledges with few kinks afford sharp dislocations. (*E* and *F*) Screw dislocations observed by in situ TMAFM under identical conditions of (*E*) R3 $Lys^{B28}Pro^{B29}$ and (*F*) R3 porcine insulin crystals. Scan size = 5 μm × 5 μm; scan rate = 2.0 Hz. The rounded dislocations in *E* signify small ΔG_k values, which are synonymous with the low surface energy for the kink planes that favors their formation.

T_6 2-Zn porcine insulin structure contains a combination of ionic, aromatic, and hydrogen-bonding forces (Baker et al., 1988). The majority of the hydrogen bonding interactions are solvent-mediated; however, a strong directional hydrogen bond exists between Thr^{B27} OH and Asp^{A18} NH of neighboring hexamers. The T_6 2-Zn porcine hexamers are stabilized further by aromatic interactions arising from the Phe^{B1} and Tyr^{A14} residues of one hexamer interacting with the Tyr^{A19} residues of a neighboring hexamer. These aromatic interactions will depend upon the conformation of the monomer (R- or T-state). In the T_6 hexamer state, all of the B1 Phe residues are situated on the periphery of the hexamer perpendicular to the crystallographic *c* axis. However, in the $T_3R_3^f$ hexamer, three of the B1 Phe residues are positioned toward the middle of the hexamer, making these less available for lateral interhexamer interaction and causing a reduction in the in-plane attachment energy associated with the growth of the (001) hexamer layers (Fig. 5).

In the $T_3R_3^f$ structure, the α-carbon carboxylate of the Thr^{B30} residue of one hexamer interacts with the guanidine side group of the Arg^{B22} residue of a neighboring hexamer. Although not a direct interaction, solvent may serve to stabilize this interface between the Thr^{B30} and Arg^{B22} residues of neighboring hexamers. Careful examination of the

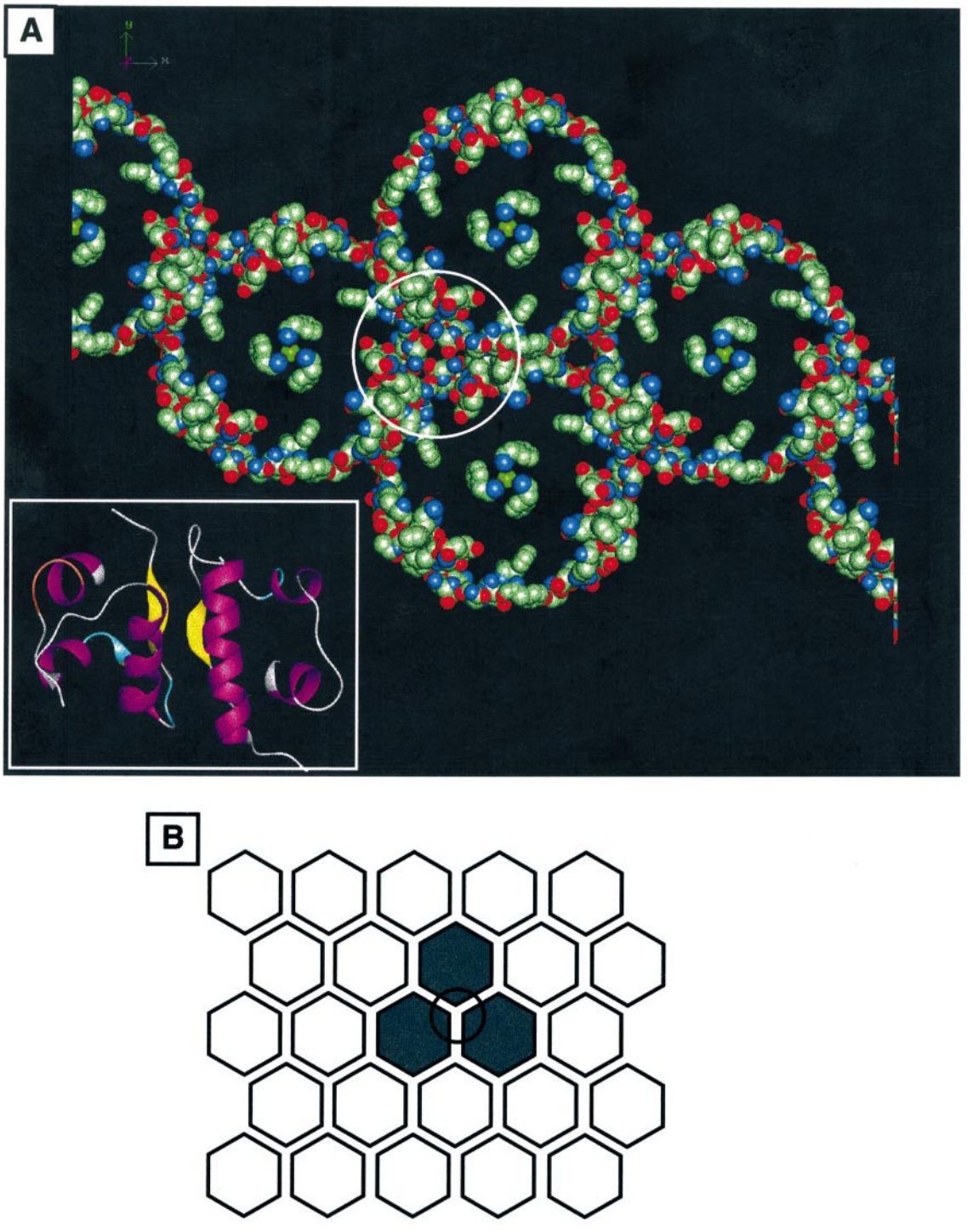

FIGURE 5 (*A*) Molecular model of the $Lys^{B28}Pro^{B29}$ hexamer packing motif in the (001) crystal plane. Only those residues involved in hexamer-hexamer contact are shown. Residues located in the middle of the hexamer rings project out of the page, and are involved in hexamer-hexamer contact with the overlying (001) crystal plane. (*Inset*) Ribbon model of $Lys^{B28}Pro^{B29}$ dimer. The models were prepared using Quanta96 (Molecular Simulations, San Diego, CA). The white outline defines the region of interhexamer contact. (*B*) Schematic model of interhexamer contacts within a hexagonal (001). The black outline corresponds to the white outline in *A*.

molecular models of $T_3R_3^f$ wild-type human insulin and $T_3R_3^f$ $Lys^{B28}Pro^{B29}$ hexamers revealed significant differences only in the B28 through B30 domains (Fig. 5). Notably, the $Lys^{B28}Pro^{B29}$ sequence restricts the free reorientation of the terminal Thr^{B30} residue, so that the Thr^{B30} group of $Lys^{B28}Pro^{B29}$ is bent away from the hexamer-hexamer contact region and resides in a relatively large solvent pocket between adjacent $Lys^{B28}Pro^{B29}$ hexamers. We note that the x-ray structure refinement for $Lys^{B28}Pro^{B29}$ yielded large thermal factors for the B29 and

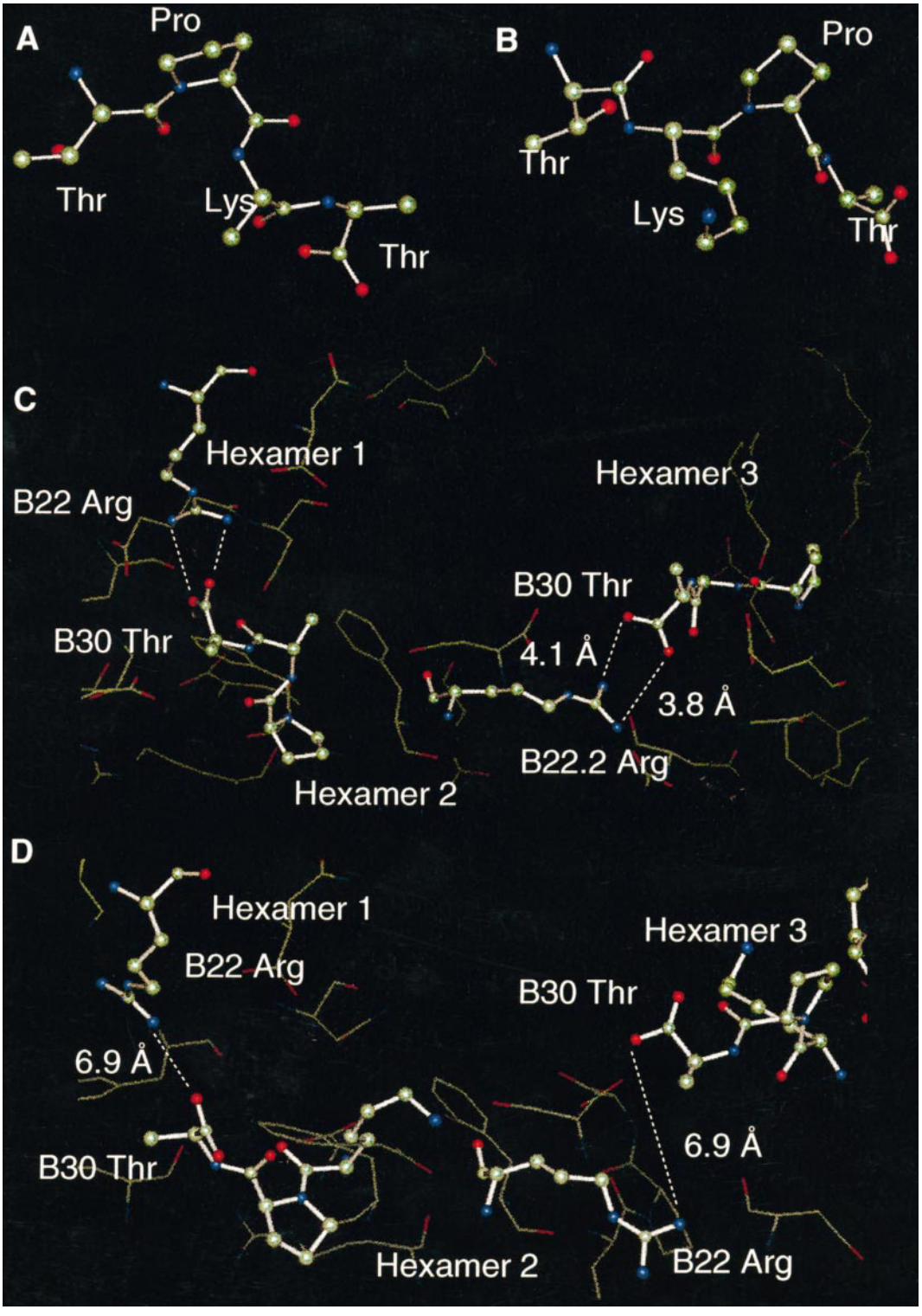

FIGURE 6 Molecular models of the $Lys^{B28}Pro^{B29}$ and human insulin $T_3R_3^f$ structure. (*A* and *B*) Models of the C-terminal B-chain B27-B30 residues of (*A*) human insulin and (*B*) $Lys^{B28}Pro^{B29}$. Because of large thermal parameters, some of the side-chain residues (e.g., lysine) were not located. (*C* and *D*) Models of the B22 Arg-B30 Thr interhexamer contacts between three neighboring hexamers of (*C*) human insulin and (*D*) $Lys^{B28}Pro^{B29}$. The B22 Arg and B28-B30 residues are shown as ball-and-stick models. The dashed lines indicate distances between the carboxylate group of the B30 Thr and the guanidine side group of the B22 Arg side chain located in the adjacent hexamer. The models were prepared with Quanta96, using coordinates registered with the Brookhaven Protein Data Bank as pdb1trz.ent (human insulin $T_3R_3^f$) and pdb1lph.ent ($Lys^{B28}Pro^{B29}$).

B30 residues (G. D. Smith, personal communication), consistent with less restricted motion in the large pocket. In the human $T_3R_3^f$ structure, the separation distance between neighboring Thr^{B30} and the Arg^{B22} groups of adjacent hexamers is ~4 Å, whereas this separation approaches 7 Å in the $Lys^{B28}Pro^{B29}$ $T_3R_3^f$ structure, (Fig. 6, *C–D*). It is reasonable to conclude that these factors will cumulatively reduce the interhexamer interaction energy in the (001) plane, thereby leading to reduced ΔG_k values that are evident from the rounded dislocation noses.

CONCLUSIONS

The studies described above provide direct insight into the influence of experimental conditions and the $Lys^{B28}Pro^{B29}$ sequence inversion on crystal growth characteristics. The bovine insulin crystals were characterized by a large number of screw and slip dislocations, in contrast with earlier AFM studies in our laboratory, in which crystal growth occurred through expansion of large (>1 μm) terraces emerging from undetectable growth centers (Yip and Ward, 1996). The crystallization conditions of this earlier work (pH 6.5–8.5, and lower concentrations of phenol) differed from those used in the present study, indicating that the crystallization medium and additives directly influence the density of screw dislocations and the structure of the solution-crystal interface.

The most remarkable observation in these studies is the substantial change in crystal growth behavior resulting from the sequence inversion at the C-terminus of the B-chain. Although the comparisons made here were for $Lys^{B28}Pro^{B29}$ and wild-type porcine/bovine insulins that have different C-terminal residues (Thr versus Ala, respectively), the considerable difference in the self-association behaviors of human and $Lys^{B28}Pro^{B29}$ insulin, which both have Thr residues at the C-terminus, suggests that the sequence inversion is principally responsible for the behavior observed by AFM. Comparison of the $Lys^{B28}Pro^{B29}$ and wild-type insulin crystal structures suggests that the sequence inversion reduces interhexamer interactions in $Lys^{B28}Pro^{B29}$, which results in a smaller attachment energy (ΔG_k) and, consequently, more rounded screw dislocations and large terrace widths. The formation of persistent vacancies in the (001) surface planes of actively growing crystals, which can result in inclusions that affect crystal quality, also can be attributed to reduced lateral interhexamer interaction. These studies demonstrate that subtle alterations in a protein sequence, designed to address a specific need such as a reduction in insulin monomer association, can influence the self-assembly into the crystalline solid state, which may (or may not) be desirable. Such considerations have significant implications for the development of novel therapeutic formulations based on crystalline protein forms.

We gratefully acknowledge Dr. G. David Smith and Dr. Ewa Ciszak of the Hauptman-Woodward Research Institute for their assistance in providing crystallization conditions and structural data.

We also acknowledge the support of the Center for Interfacial Engineering, a National Science Foundation Engineering Research Center.

REFERENCES

Abola, E. E., F. C. Bernstein, S. H. Bryant, T. F. Koetzle, and J. Weng. 1987. Protein Data Bank. *In* Crystallographic Databases—Information Content, Software Systems, Scientific Applications. F. H. Allen, G. Bergerhoff, and R. Sievers, editors. Data Commission of the International Union of Crystallography, Bonn, Cambridge, Chester. 107–132.

Bakaysa, D. L., J. Radziuk, H. A. Havel, M. L. Brader, S. L. Edwards, S. W. Dodd, J. M. Beals, A. H. Pekar, and D. N. Brems. 1996. Physiochemical basis for the rapid time-action of $Lys^{B28}Pro^{B29}$-insulin: dissociation of a protein-ligand complex. *Protein Sci.* 5:2521–2531.

Baker, E. N., T. L. Blundell, J. F. Cutfield, S. M. Cutrfield, E. J. Dodson, G. G. Dodson, D. M. Crowfoot Hodgkin, R. E. Hubbard, N. W. Isaacs, C. D. Reynolds, K. Sakabe, N. Sakabe, and N. Vijayan. 1988. The structure of 2Zn pig insulin crystals at 1.5 Å resolution. *Philos. Trans. R. Soc. Lond. Biol.* 319:369–456.

Bernstein, F. C., T. F. Koetzle, G. J. B. Williams, E. F. Meyer, Jr., M. D. Brice, J. R. Rodgers, O. Kennard, T. Shimanouchi, and M. Tasumi. 1977. The Protein Data Bank: a computer-based archival file for macromolecular structures. *J. Mol. Biol.* 112:535–542.

Berson, S. A., and R. S. Yalow. 1966. Insulin in blood and insulin antibodies. *Am. J. Med.* 40:676–690.

Birnbaum, D. A., M. A. Kilcomons, M. R. DeFelippis, and J. M. Beals. 1997. Assembly and dissociation of human insulin and $Lys^{B28}Pro^{B29}$-insulin hexamers: a comparison study. *Pharm. Res.* 14:25–36.

Bohindar, H. B., and E. Geissler. 1984. Static and dynamic light scattering from dilute insulin solutions. *Biopolymers.* 23:2407–2417.

Brange, J., G. G. Dodson, and B. Xiao. 1991. Designing insulin for diabetes therapy by protein engineering. *Curr. Opin. Struct. Biol.* 1:934–940.

Brange, J., D. R. Owens, S. Kang, and A. Volund. 1990. Monomeric insulins and their experimental and clinical implications. *Diabetes Care.* 13:923–954.

Brems, D. N., L. A. Alter, M. J. Beckage, R. E. Chance, R. D. DiMarchi, L. K. Green, H. B. Long, A. H. Pekar, J. E. Shields, and B. H. Frank. 1992a. Altering the association properties of insulin by amino acid substitution. *Protein Eng.* 5:527–533.

Brems, D. N., P. L. Brown, C. Bryant, R. E. Chance, L. K. Green, H. B. Long, A. A. Miller, R. Millican, J. E. Shields, and B. H. Frank. 1992b. Improved insulin stability through amino acid substitution. *Protein Eng.* 5:519–525.

Carstensen, J. T. 1977. Pharmaceutics of Solids and Solid Dosage Forms. John Wiley and Sons, New York.

Carter, P. W., A. C. Hillier, and M. D. Ward. 1994. Nanoscale surface topography and growth of molecular crystals: the role of anisotropic intermolecular bonding. *J. Am. Chem. Soc.* 116:944–953.

Ciszak, E., J. M. Beals, B. H. Frank, J. C. Baker, N. D. Carter, and G. D. Smith. 1995. Role of C-terminal B-chain residues in insulin assembly: the structure of hexameric $Lys^{B28}Pro^{B29}$-human insulin. *Structure.* 3:615–622.

Ciszak, E., and G. D. Smith. 1994. Crystallographic evidence for dual coordination about zinc in the T3R3 human insulin hexamer. *Biochemistry.* 33:1512–1517.

DiMarchi, R. D., J. P. Mayer, L. Fan, D. N. Brems, B. H. Frank, L. K. Green, J. A. Hoffman, D. C. Howey, H. B. Long, W. N. Shaw, J. E. Shields, L. J. Slieker, K. S. E. Su, K. L. Sundell, and R. E. Chance. 1992. Synthesis of fast acting insulin based on structural homology with insulin-like growth factor I. *In* Peptides: Chemistry and Biology, Proceedings of the Twelfth American Peptide Symposium, ESCOM, Leiden. J. E. Smith and J. E. Rivier, editors. 26–28.

Durbin, S. D., and W. E. Carlson. 1992. Lysozyme crystal growth studied by atomic force microscopy. *J. Cryst. Growth.* 122:71–79.

Durbin, S. D., W. E. Carlson, and M. T. Saros. 1993. In situ studies of protein crystal growth by atomic force microscopy. *J. Phys. D Appl. Phys.* 26:B128–B132.

Durbin, S. D., and G. Feher. 1990. Studies of crystal growth mechanisms of proteins by electron microscopy. *J. Mol. Biol.* 212:763–774.

Gammeltoft, S. 1988. Insulin Receptors, Part A: Methods for the Study of Structure and Function. C. R. Kahn and L. C. Harrison, editors. Allan R. Liss, New York.

Hansma, P. K., J. P. Cleveland, M. Radmacher, D. A. Walters, P. E. Hillner, M. Bezanilla, M. Fritz, D. Vie, H. G. Hansma, C. R. Prater, J. Massie, L. Fukunaga, J. Gurley, and V. Elings. 1994. Tapping mode atomic force microscopy in liquids. *Appl. Phys. Lett*. 64:1738–1740.

Hillier, A. C., J. B. Maxson, and M. D. Ward. 1994. Electrocrystallization of an ordered organic monolayer: selective epitaxial growth of β-$(ET)_2I_3$ on graphite. *Chem. Mater.* 6:2222–2226.

Hillier, A. C., and M. D. Ward. 1994. Atomic force microscopy of the electrochemical nucleation and growth of molecular crystals. *Science.* 263:1261–1264.

Hollenberg, M. D. 1990. Receptor triggering and receptor regulation: structure-activity relationships from the receptor's point of view. *J. Med. Chem.* 33:1275–1281.

Howey, D. C., R. R. Bowsher, R. L. Brunelle, and J. R. Woodworth. 1994. [Lys(B28), Pro(B29)]-human insulin: a rapidly absorbed analogue of human insulin. *Diabetes.* 43:396–402.

Hvidt, S. 1991. Insulin association in neutral solution studied by light scattering. *Biophys. Chem.* 39:205–213.

Jeffrey, P. D. 1974. Polymerization behavior of bovine-zinc insulin at neutral pH. Molecular weight of the subunit and the effect of glucose. *Biochemistry.* 13:4441–4447.

Kaarsholm, N. C., H.-C. Ko, and M. F. Dunn. 1989. Comparison of the solution structure flexibility and zinc binding domains for insulin, proinsulin and miniproinsulin. *Biochemistry.* 28:4427–4435.

Kadima, W., A. McPherson, M. F. Dunn, and F. A. Jurnak. 1991. Precrystallization aggregation of insulin by dynamic light scattering and comparison with canavalin. *J. Cryst. Growth.* 110:188–194.

Konnert, J. H., P. D'Antonio, and K. B. Ward. 1994. Observations of growth steps, spiral dislocations and molecular packing on the surface of lysozyme crystals with the atomic force microscope. *Acta Crystallogr.* D50:603–613.

Kuznetsov, Y. G., A. J. Malkin, W. Glantz, and A. McPherson. 1996. In situ atomic force microscopy studies of protein and virus crystal growth mechanisms *J Crystal Growth.* 168:63–73.

LaGraff, J. R., and A. A. Gewirth. 1994. Enhanced electrochemical deposition with an atomic force microscope. *J. Phys. Chem.* 98: 11246–11250.

LaGraff, J. R., and A. A. Gewirth. 1995. Nanometer-scale mechanism for the constructive modification of Cu single crystals and alkanethiol passivated Au(111) with an atomic force microscope. *J. Phys. Chem.* 99:10009–10018.

Land, T. J., A. J. Malkin, Y. G. Kuznetsov, A. McPherson, and J. J. De Yoreo. 1995. Mechanisms of protein crystal growth: an atomic force microscopy study of canavalin crystallization. *Phys. Rev. Lett.* 75: 2774–2777.

Land, T. J., A. J. Malkin, Y. G. Kutznesov, A. McPherson, and J. J. DeYoreo. 1996. Mechanisms of protein and virus crystal growth: an atomic force microscopy study of canavalin and STMV crystallization. *J. Crystal Growth.* 166:893–899.

Last, J. A., and M. D. Ward. 1996. Electrochemical annealing and friction anisotropy of domains in epitaxial molecular films. *Adv. Mater.* 8:730–733.

Long, H. B., J. C. Baker, R. M. Belagaje, R. D. DiMarchi, B. H. Frank, L. K. Green, J. A. Hoffman, W. L. Muth, A. H. Pekar, S. G. Reams, W. N. Shaw, J. E. Shields, L. J. Slieker, K. S. E. Su, K. L. Sundell, and R. E. Chance. 1992. Human insulin analogs with rapid onset and short duration of action. *In* Peptides: Chemistry and Biology, Proceedings of the Twelfth American Peptide Symposium, ESCOM, Leiden. J. E. Smith and J. E. Rivier, editors. 88–90.

Malkin, A. J., Yu. G. Kuznetsov, and A. McPherson. 1996. Defect structure in macromolecular crystals. *J. Struct. Biol.* 117:124–137.

Malkin, A. J., T. J. Land, Y. G. Kuznetsov, A. McPherson, and J. J. De Yoreo. 1995. Investigation of virus crystal growth mechanisms by in-situ atomic force microscopy. *Phys. Rev. Lett.* 75:2778–2781.

Manne, S., J. P. Cleveland, G. D. Stucky, and P. K. Hansma. 1993. Lattice resolution and solution kinetics on surfaces of amino acid crystals: an atomic force microscope study. *J. Crystal Growth.* 130:333–340.

Mao, G., L. Lobo, R. Scaringe, and M. D. Ward. 1997. Nanoscale visualization of crystal habit modification by atomic force microscop. *Chem. Mater.* 9:773–783.

McPherson, A., A. J. Malkin, Y. G. Kuznetsov, and S. Koszelak. 1996. Incorporation of impurities into macromolecular crystals. *J. Crystal Growth.* 168:74–92.

Milthorpe, B. K., L. W. Nichol, and P. D. Jeffrey. 1977. The polymerization pattern of zinc(II)-insulin at pH 7.0. *Biochim. Biophys. Acta.* 495: 195–202.

Ng, J. D., Y. G. Kuznesov, A. J. Malkin, G. Keith, R. Geige, and A. McPherson. 1997. Visualization of RNA crystal growth by atomic force microscopy. *Nucleic Acids Res.* 25:2582–2588.

Pederson, J. S., S. Hansen, and R. Bauer. 1994. The aggregation behavior of zinc-free insulin studied by small-angle neutron scattering. *Eur. Biophys. J.* 22:379–389.

Smith, G. D., D. C. Swenson, E. J. Dodson, G. G. Dodson, and C. D. Reynolds. 1984. Structural stability in the 4-zinc human insulin hexamer. *Proc. Natl. Acad. Sci. USA.* 81:7093–7097.

Tiller, W. A. 1991. The Science of Crystallization: Microscopic Interfacial Phenomena. Cambridge University Press, Cambridge.

Tiller, W. A. 1992. The Science of Crystallization: Macroscopic Phenomena, and Defect Generation. Cambridge University Press, Cambridge.

Yip, C. M., and M. D. Ward. 1996. Atomic force microscopy of insulin single crystals: direct visualization of molecules and crystal growth. *Biophys. J.* 71:1071–1078.